Variable-height scanning tunneling spectroscopy for local density of states recovery based on the one-dimensional WKB approximation

B. Naydenov* and John J. Boland
School of Chemistry and Center for Research on Adaptive Nanostructures and Nanodevices (CRANN), Trinity College Dublin, Dublin 2, Ireland

(Received 10 September 2010; revised manuscript received 16 October 2010; published 9 December 2010)

We introduce a variable-height scanning tunneling spectroscopy (VH-STS) method that provides a good level of recovery of the combined surface and tip density of states (DOS) in any bias range without the complexity of previous methods. The combined local electron DOS (LDOS) recovery was performed using a simplified algorithm based on the one-dimensional Wentzel-Kramers-Brillouin approximation already known in the literature. On the basis of this VH-STS approach we derive three separate methods for the determination of tunnel barrier height and absolute tip-surface separation, and which are critical to enabling LDOS recovery. We report experimental results on polycrystalline-Pt and Si(100) surfaces using this scheme. Experimental and simulated spectra are compared to investigate the limits of the various methods and to demonstrate that this approach can be applied successfully to all kind of probes and surfaces.

DOI: 10.1103/PhysRevB.82.245411 PACS number(s): 68.37.Ef, 73.20.At

I. INTRODUCTION

Spectroscopy with atomic resolution has been one of the most attractive and challenging outcomes of the invention of the scanning tunneling microscope (STM).[1] The accuracy and reproducibility of the acquired scanning tunneling spectroscopic (STS) data have improved dramatically since the development of the cryogenic STM. Despite the fact that the local electron density of states (LDOS) has been the main STS objective, until recently there were no significant theoretical efforts to recover this fundamental property from STS measurements of the tunneling current $I(V)$ and differential conductance $dI(V)/dV$. The quantity $(dI/dV)/(I/V)$ (Ref. 2) is still widely used as an estimate of the LDOS although it is clear that it is a rather poor approximation[3] and is not tip-sample distance invariant contrary to recent reports.[4] In the past several years there were significant theoretical studies[5–12] involving schemes for LDOS deconvolution from the STS data based on the one-dimensional Wentzel-Kramers-Brillouin (1D-WKB) approximation. These algorithms, recently summarized by Passoni *et al.*[11] have led to a better understanding of the STS experiment but they have not yet been widely adopted in the experimental studies.[13] The reason for this is the considerable computational effort required coupled with the need for very accurate data and the fact that a knowledge of two nondirectly measurable quantities (tunneling barrier height and absolute tip-surface separation) are required for LDOS recovery. Thus to benefit from the full potential of the recovery scheme efforts should be made to acquire good quality data over the entire energy range and to develop a simple and fast data processing procedures for parameter determination.

Here we introduce and describe a variable-height scanning tunneling spectroscopy (VH-STS) scheme which has the particular advantage that it allows the signal-to-noise ratio to be adjusted over the entire measured energy range. The VH-STS serves as platform for a procedure to obtain the combined tip-sample LDOS recovery based on the 1D-WKB theory. Based on the VH-STS approach we derive (Sec. III) three separate methods (Φ^*, z^*, and $\Delta R_{1,2}$ methods) for the determination of tunneling barrier and tunneling distance, which, in turn, provide separate information about the tip and the sample electronic structures. We test the limits of these various methods and the recovery scheme, in general, on simulated (Sec. IV) and experimental data (Sec. V). We demonstrate that the $\Delta R_{1,2}$ method is applicable to all type of probes and surfaces and provides a topographic map with a directly observable local minimum calculated from spectroscopic data at a single-bias value. This minimum provides an accurate estimate of both the work function and the absolute tip-sample separation which are critical for combined LDOS recovery and clearly distinguishes our approach from similar methods published in the literature.[10–12] The Φ^* and z^* methods, although not applicable to all samples and probes, still provide very useful information about underlying surface phenomena and probe electronic structure which can be used for data modeling (Sec. VI) and ultimately to isolate the surface LDOS from the combined tip and sample LDOS.

II. EXPERIMENTAL LAYOUT

Experiments were performed using a Createc cryogenic STM operating at 5 and 77 K. The UHV system includes: analysis, preparation, and load-lock chambers with base pressures $<1\times10^{-11}$ mbar, 2×10^{-11} mbar, and 6×10^{-11} mbar, respectively. A cryogenic manipulator provided controlled conditions throughout the whole process of sample preparation and transfer to the microscope. Metal (polycrystalline Pt) and semiconductor [Si(100)n+] samples were mounted on a dual-sample holder shown in Fig. 1(a). Access to both surfaces is provided in the microscope without sample exchange. Both samples can be prepared separately and topographic images demonstrating the quality of the surfaces are presented also in Figs. 1(b) and 1(c).

Tungsten probes ware annealed *in situ* and inked[14] on the metal surface in the microscope. The spatial stability of the microscope (<1 pm/min in XYZ) provided the necessary conditions for the acquisition of few minutes long spectra

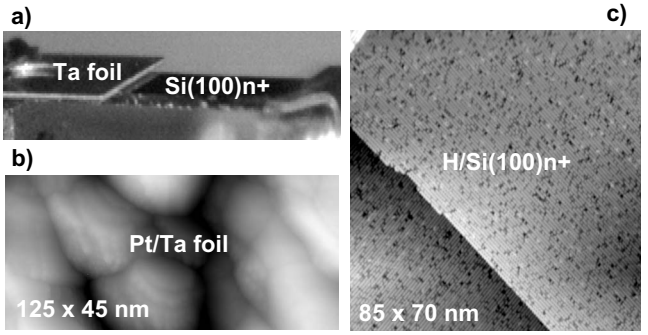

FIG. 1. Sample holder configuration and sample preparation. (a) shows two different samples for STM/STS without sample exchange. (b) is topographic image of the first surface (polycrystalline Pt) recorded with tunneling current of 100 pA and sample bias of 2 V. (c) shows topographic image of the second sample obtained with current 50 pA and sample bias −2 V representing Si(100) surface decorated with atomic hydrogen.

with the feedback off. The spectroscopy was performed by choosing a spatial set point, switching the feedback off and ramping the bias (V) and the tip-sample separation (z) through a set of programmed values while recording simultaneously the tunneling current and its derivative over the bias. An external lock-in amplifier was used for the bias modulation (590 Hz, 20 mV rms) and the current derivative detection. In every spectrum the bias and the separation were changed forward and backward to ensure that no time hysteresis exists in the recorded channels. Prior to the spectroscopy measurement key values for the tip-sample separation were obtained by simultaneous multiple-bias imaging of the surface area under investigation so as to define the tip-sample-bias spectroscopic trajectories. These z values were then programmed in the VH-STS parameters together with the corresponding biases. The latter was sufficient to avoid any tip and/or surface modifications during the experiment. All experiments were performed at liquid-nitrogen temperatures.

III. THEORETICAL LAYOUT

In the scanning tunneling spectroscopy the principally measured quantity is the tunneling current $I(V)$ which is commonly expressed[5–12] in the form

$$I(V) \propto \int_0^{eV} \rho_S(\varepsilon)\rho_t(\varepsilon - eV)T(\varepsilon, eV, z)d\varepsilon, \tag{1}$$

where $\boldsymbol{\rho}_S$ and $\boldsymbol{\rho}_t$ are the sample and tip LDOSs, respectively, $\mathbf{V}$ is the bias, and $\mathbf{z}$ is the separation between the sample and the probe. $\mathbf{T}$ is the barrier transmission coefficient which in the 1D-WKB trapezoidal approximation can be expressed as

$$T(\varepsilon, eV, z) = \exp\left(-\alpha z\sqrt{\Phi + \frac{eV}{2} - \varepsilon}\right). \tag{2}$$

Here $\boldsymbol{\Phi}$ is the tunneling barrier height and $\alpha = 2\sqrt{2m}/\hbar$.

Following Koslowski *et al.*[7,10] the second STS quantity, namely, the differential conductance $dI/dV(V)$ can be derived from Eqs. (1) and (2) and applying the mean-value theorem for integrals it has the form

$$\frac{dI(V)}{dV} = \rho_S(V)\rho_t(0)T(eV, eV, z) - \frac{\alpha z}{\beta\sqrt{\Phi}}I(V) + \int_0^{eV} \rho_S(\varepsilon)T(\varepsilon, eV, z)\frac{d\rho_t(\varepsilon - eV)}{dV}d\varepsilon, \tag{3}$$

where the constant $\beta \approx 4$.[7] Equation (3) can be rearranged as follows:

$$\rho_S(V)B_T = \left[\frac{dI(V)}{dV} + \frac{\alpha z}{\beta\sqrt{\Phi}}I(V)\right]/T(eV, eV, z), \tag{4}$$

where B_T is given by

$$B_T = \rho_t(0) + \int_0^{eV} P_{S,T}(\varepsilon, eV)\frac{d\rho_t(\varepsilon - eV)}{dV}d\varepsilon \tag{5}$$

and

$$P_{S,T}(\varepsilon, eV) = \frac{\rho_S(\varepsilon)}{\rho_S(V)}\frac{T(\varepsilon, eV, z)}{T(eV, eV, z)}. \tag{6}$$

If $\rho_S(\varepsilon)$ is changing slowly compared with the exponent $T(\varepsilon)$ then one can make the approximation

$$P_{S,T}(\varepsilon, eV) \cong \text{const.} = 1. \tag{7}$$

Additionally if we replace $d\rho_t(\varepsilon - eV)/dV$ with $-d\rho_t(\varepsilon - eV)/d\varepsilon$ in Eq. (5), this equation is reduced to $B_T \cong \rho_t(-V)$ and Eq. (4) can then be rewritten as

$$\rho_{S,t}(V) = \rho_S(V)\rho_t(-V) \cong \left[\frac{dI(V)}{dV} + \frac{\alpha z}{\beta\sqrt{\Phi}}I(V)\right]/T(eV, eV, z). \tag{8}$$

For a tip with a flat LDOS the left-hand side of Eq. (8) becomes $\rho_S(V)\rho_t(0)$ as described earlier in the work of Koslowski *et al.*[7] On the right-hand side of Eq. (8) the key unknown parameters are the separation $\mathbf{z}$ and the barrier height $\boldsymbol{\Phi}$. Koslowski *et al.*[10] demonstrated that measurements with two significantly different separations can be used as a basis for the tip and sample LDOS recovery by solving a set of integrodifferential equations employing the Neumann approximation scheme. Here we suggest instead that $\mathbf{z}$ and $\boldsymbol{\Phi}$ can be determined by applying only Eq. (8) for two variable-height scanning tunneling spectra measuring $I(V)$ and $dI/dV(V)$. If the absolute separation is z_0 and defined for a given bias V_0 and current I_0 one can design two measurements using predetermined separations $z_1(V) = z_0 + \Delta z_1(V)$ and $z_2(V) = z_0 + \Delta z_2(V)$. The four acquired spectra, $I(V)$ and $dI/dV(V)$ measured at z_1 and z_2 are expected to give equal products when applied in Eq. (8), namely, the recovered LDOS should be identical for measurements at both separations

$$\rho_{S,t}(V, z_1) \equiv \rho_{S,t}(V, z_2). \tag{9}$$

At zero bias ($V = 0$) the current is zero and one can determine from Eqs. (8) and (9) that the barrier height is given by

$$\Phi = \Phi^*(0) = \left\{ \ln\left[\frac{dI_1(0)}{dV} / \frac{dI_2(0)}{dV} \right] / [\alpha \Delta z(0)] \right\}^2. \quad (10)$$

Here $\Delta z(V) = z_2(V) - z_1(V) = \Delta z_2(V) - \Delta z_1(V)$ is the predetermined separation difference between the two spectra at given bias. The obtained value of $\mathbf{\Phi}$ could be verified by comparison with the apparent barrier $\mathbf{\Phi_A}$ for small biases having the form $\Phi_A(V) = \{\ln[I_1(V)/I_2(V)]/[\alpha \Delta z(V)]\}^2$ but this comparison is not always possible as we will show later in Sec. V. The Φ^* method based on Eq. (10) for $\mathbf{\Phi}$ acquisition is expected to be superior to the apparent barrier measurements $\mathbf{\Phi}_A(V)$ due to the nonzero values of dI/dV at zero bias which is usually the case for the commonly used STM samples (degenerately doped semiconductors and metals). Additionally in the experiment the current derivative is recorded using lock-in amplifier which has high sensitivity even for currents in the picoampere range.

After obtaining the barrier $\mathbf{\Phi}$ from Eq. (10) one can solve Eq. (9) for the absolute separation z_0

$$z^*(V) = z_0(V) = \frac{P_3 \frac{dI_2(V)}{dV} - \frac{dI_1(V)}{dV} + P_2 P_3 \Delta z_2 - P_1 \Delta z_1}{P_1 - P_2 P_3}, \quad (11)$$

where $P_1 = \alpha I_1(V)/(\beta\sqrt{\Phi})$, $P_2 = \alpha I_2(V)/(\beta\sqrt{\Phi})$, and $P_3 = \exp[\alpha \Delta z(V)\sqrt{\Phi - V/2}]$. Equation (11) should be sufficient to obtain the absolute separation value because all parameters on the right-hand side are known from the experimental design and measurement plus the tunneling barrier value is calculated with Eq. (10). To verify the result of this z^* method one can approach the surface up to a point contact but the accuracy of the latter method depends on the tip and surface materials and can vary from +0.5 to +2 Å due to strong surface-tip force gradient and a tendency for atoms to hop from the tip to sample or vice versa.[15]

An alternative method for simultaneous determination of the tunneling barrier height and absolute tip-sample separation is based on finding a local minimum of the $\Delta R_{1,2}$ product obtained from the VH-STS and by independently varying $\mathbf{\Phi}$ and z_0. The form of this product is defined as

$$\Delta R_{1,2} = |1 - \rho_{S,t}(V,z_1)/\rho_{S,t}(V,z_2)|, \quad (12)$$

where $\boldsymbol{\rho}_{S,t}(V,z_1)$ and $\boldsymbol{\rho}_{S,t}(V,z_2)$ are obtained by applying Eq. (8) to $I(V)$ and $dI/dV(V)$ spectra with corresponding z_1 and z_2 separations. The difference between this method and that proposed by Koslowski *et al.*[10] is that it provides a topographic map showing a local minimum defined by $\mathbf{\Phi}$ and z_0 that is calculated from experimental data recorded at a single-bias value. We will apply this $\Delta R_{1,2}$ method on simulated (Sec. IV) and experimental data (Sec. V) and will demonstrate that in the physically meaningful 3–6 eV and 2–12 Å ranges for Φ and z_0, respectively, there always exists a local minimum that allows for accurate $\mathbf{\Phi}$ and z_0 determination. The $\Delta R_{1,2}$ method should be viewed as complimentary to the Φ^* and z^* methods and for some tip-sample systems (Sec. V) we will show that it is the only applicable method to acquire accurate Φ and z_0 values.

As discussed earlier, the parameter β has a value close to 4 but Koslowski *et al.*[7] by applying second-order approximation for tip with a flat constant LDOS acquired β as function of V, Φ, and z. This function[7] with one slightly modified parameter is given here as

$$\beta(V,\Phi,z) = 4\left[1 + \frac{(2z_0\sqrt{\Phi} + 3)V^2}{98\Phi^2} \right]^{-1}. \quad (13)$$

The corrected value of β has a dependence on z_0 which means that it is possible to iterate Eqs. (11) and (13) in sequence by starting with $\beta = 4$. In the simulation part of this study (Sec. IV) we will investigate the influence of this correction [Eq. (13)] on the recovered LDOS spectra.

The complimentary Φ^*, z^*, and $\Delta R_{1,2}$ methods based on Eqs. (10)–(12), respectively, provide the complete set of parameters required in Eq. (8) and the combined sample and tip LDOSs can be recovered at the corresponding VH-STS position on the surface. Still to obtain the sample LDOS one must know the tip LDOS which can be determined by measurements on surfaces with known LDOS, by modeling (as applied in this work in Sec. VI) or by applying the fitting methods reviewed in Ref. 11. Generally a good STM probe is expected to have flat and featureless LDOS which means that the convoluted spectrum yielded by Eq. (8) will reflect with high accuracy the sample LDOS multiplied by factor $\boldsymbol{\rho}_t(\mathbf{0})$, except probably for the high negative sample-bias region[11] where the β correction [Eq. (13)] can help improve the accuracy (see Sec. IV, below).

IV. SIMULATIONS

As a proof of concept for the VH-STS scheme and to investigate the behavior of the Φ^*, z^*, and $\Delta R_{1,2}$ methods for the $\mathbf{\Phi}$ and z_0 acquisition we simulated several cases of sample and probe density of states ranging from metal to semiconductor surfaces.

A. Flat $\boldsymbol{\rho}_S = \boldsymbol{\rho}_t$

We start our simulations with the simplest case of a constant $\boldsymbol{\rho}_S = \boldsymbol{\rho}_t = 30$ mS and with parameters: $z_0 = 8$ Å, $\Delta z_1 = 0$ Å, $\Delta z_2 = 0.3$ Å, and $\mathbf{\Phi} = 5.35$ eV. The calculated currents and their derivatives over the bias are presented in Figs. 2(a) and 2(b), respectively, with black lines for $z_1 = z_0 + \Delta z_1$ and red lines for $z_2 = z_0 + \Delta z_2$. The $\mathbf{\Phi}^*$ spectrum (black line) applying Eq. (10) and the apparent barrier height $\mathbf{\Phi}_A$ using the current values (blue line) are shown in Fig. 2(c). Both spectra approach a value of 5.35 eV at small biases demonstrating the consistency of the two methods. In the Fig. 2(d) the $z^*(V)$ curve is plotted and shows a monotonic dependence reaching the z_0 value at $V = 0$. We have used $\beta = 4$ because in the sequence of operations in the scheme no knowledge of z_0 is available at this point. The nonconstant $z^*(V)$ spectrum reflects the fact that $\beta = 4$ is used but still a simple parabolic fit gives the correct z_0 value at $V = 0$. As we will demonstrate later for more complex LDOSs the $z^*(V)$ cannot be fitted with a parabola and one could physically bring the tip into contact with the sample to determine z_0. Alternatively, the $\Delta R_{1,2}(V)$ method can be applied and in Fig.

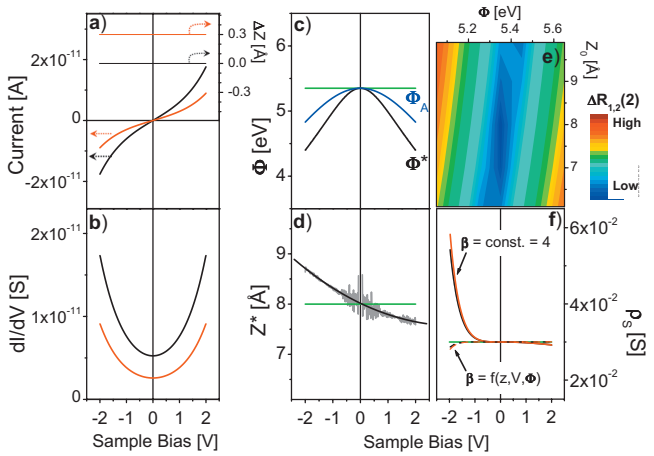

FIG. 2. (Color) Simulated VH-STS data for tip and surface both with flat and equal electron density of states. Black and red colors correspond to z_1 and z_2, respectively. The parameters used are $\rho_S=\rho_t=30$ mS, $z_0=8$ Å, $\mathbf{\Phi}=5.35$ eV, $\Delta z_1=$const.$=0$ Å, and $\Delta z_2=$const.$=0.3$ Å. Tunneling currents are plotted in (a) and their bias derivatives are plotted in (b). In (c) $\Phi^*(V)$, $\Phi_A(V)$, and $\mathbf{\Phi}$ are shown as black, blue, and green curves, respectively. The grey spectrum in (d) is $z^*(V)$ and black shows the parabolic fit to this curve. The green line indicates the z_0 value in (d). (e) shows the intensity map of $\Delta R_{1,2}$ at 2 V as a function of $\mathbf{\Phi}$ and z_0. In (f) the recovered surface LDOS is shown with solid lines for $\beta=4$ and dashed lines using β determined from Eq. (13). The original input ρ_S is shown in green.

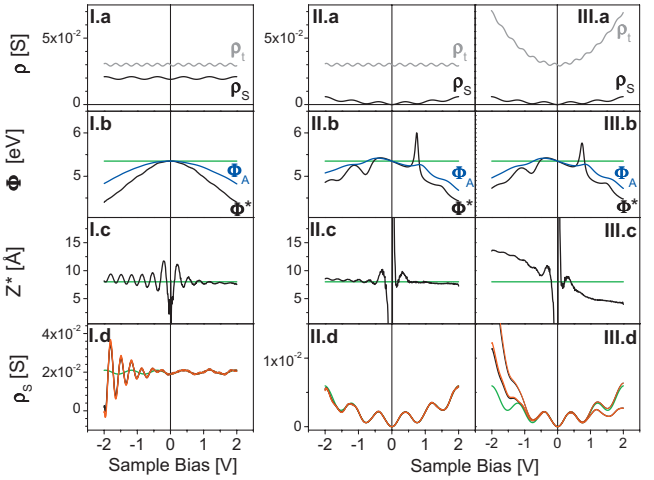

FIG. 3. (Color) Simulated VH-STS data for complex nonequal tip and surface electron density of states. The results for three (I)–(III) cases are organized in columns of panels. The parameters used are as in Fig. 2 except for ρ_S and ρ_t. For all cases modulation with a cosine (amplitude 1 mS, period 0.3 V, and phase $\pi/2$) is added to the tip LDOS, which is a flat 30 mS background [in (I) and (II)] and parabolic [in (III)] background. Constant cosine modulation (amplitude 1 mS, period 0.8 V, and phase π) is added in all cases to the surface LDOS, which is a flat 20 mS background in (I) and parabolic backgrounds in (II) and (III), where the latter are shifted vertically to equal zero intensity at $V=0$. The tip and sample LDOS inputs are plotted in panels (a) for the corresponding columns of simulated data. In the (b) panels $\Phi^*(V)$, $\Phi_A(V)$, and $\mathbf{\Phi}$ are shown in black, blue, and green, respectively. The black curves in panels (c) are $z^*(V)$ spectra while in green is the constant $z_0=8$ Å value for all three cases. In black for z_1 and red for z_2 the recovered surface LDOSs are shown in panels (d) together with the input ρ_S in green for the corresponding three cases. In the (d) panels solid lines are applied for the recovery products $\rho_{S,t}(V)/\rho_t(0)$ and dashed lines for $\rho_{S,t}(V)/\rho_t(-V)$.

2(e) a map of $\Delta R_{1,2}(2)$ is plotted against variables Φ and z_0. One can readily detect the local minimum at $\mathbf{\Phi}=5.35$ eV and $z_0=8$ Å. Thus finding the minimum in Fig. 2(e) demonstrates an additional method to determine the barrier height and the absolute separation. From our point of view this variety of methods represents a self-consistent basis for reliable $\mathbf{\Phi}$ and z_0 determination.

Finally, the $\boldsymbol{\rho}_S(V)$ is obtained by dividing $\boldsymbol{\rho}_{S,t}(V)$ by $\boldsymbol{\rho}_t$ and is presented in Fig. 2(f) with black curves for z_1 and red curves for z_2. Solid and dashed lines are applied in Fig. 2(f) to distinguish between the results obtained with $\beta=4$ and $\beta=f(z,\Phi,V)$, respectively. It is obvious from the plot that applying Eq. (13) for β results in significant reduction in the discrepancy at the high negative biases and demonstrates a good recovery of the generated LDOS.

B. Complex $\boldsymbol{\rho}_S \neq \boldsymbol{\rho}_t$

Next we investigate three separate cases with more complex density of states for both the sample and the probe. Different modulations are applied to both $\boldsymbol{\rho}_S$ and $\boldsymbol{\rho}_t$ to help investigate their separate influences on the $\mathbf{\Phi}^*(V)$, $z^*(V)$, and $\boldsymbol{\rho}_{S,t}(V)$ spectra. We have kept the simulation parameter as in the previous case, namely: $z_0=8$ Å, $\Delta z_1=0$ Å, $\Delta z_2=0.3$ Å, and $\mathbf{\Phi}=5.35$ eV for the all three cases. For all recovered $\boldsymbol{\rho}_S(V)$ spectra we used β defined by Eq. (13). A cosine modulation width amplitude of 1 mS is applied to a density of states background with period 0.8 V and phase π for the sample and period 0.3 V and phase $\pi/2$ for the tip. The different periods of the modulations are chosen to help distinguish between the influences of the surface and probe LDOS in the final product of the recovery scheme. In panels (a) of Fig. 3 the generated $\boldsymbol{\rho}_S$ and $\boldsymbol{\rho}_t$ for the three cases are plotted. In case (I) [see Fig. 3, (Ia)] a model of metal surface and metal tip is presented with constant backgrounds of 20 mS and 30 mS, respectively. In case (II) [see Fig. 3, (IIa)] the surface background is slightly parabolic and reduced to open a gap around $V=0$, thus modeling a semiconductor surface. The tip LDOS is kept unchanged. In case (III) [see Fig. 3, (IIIa)] the sample is again a semiconductor as in case (II) but the tip background is changed to become parabolic.

After calculating the currents and their derivatives for z_1 and z_2 we applied Eq. (10) for the derivatives ($\mathbf{\Phi}^*$—black curves) and the currents ($\mathbf{\Phi}_A$—blue curves) and the resulting spectra are presented in the panels (b) of Fig. 3 for the corresponding cases organized in columns of panels. For the metal surface [see Fig. 3, (Ib)] both spectra are relatively smooth parabolas and approach the true barrier value at $V=0$. The spectra are symmetric for positive and negative biases. For the semiconductor surface [see Fig. 3, (IIb) and (IIIb)] the spectra are strongly modulated with a period similar to the surface LDOS but still approach the correct value of the tunneling barrier at small biases. The curves on the

negative-bias range are shifted to higher values in comparison with positive-bias range. In all three cases the $\mathbf{\Phi}^*$ method [Eq. (10)] is applicable for the correct tunneling barrier determination.

The next step is to test how the z^* method recovers the absolute separation. The corresponding $z^*(V)$ spectra for each case derived using Eq. (11) and $\beta=4$ are shown in the panels (c) of Fig. 3. In the case of the metal surface [see Fig. 3, (Ic)] a linear curve is strongly modulated with a period similar to modulation of tip LDOS. This corrugation is significantly reduced in amplitude in the cases of the semiconductor surface [see Fig. 3, (IIc) and (IIIc)]. The linear background of $z^*(V)$ is altered in case (III) [see Fig. 3, (IIIc)] reflecting the changed tip LDOS. For all three cases a linear or simple polynomial fit can be used to acquire the correct z_0 value by extrapolation to $V=0$.

The results from the $\Delta R_{1,2}$ method applied to the three cases in Fig. 3 are not shown because they are identical with the result for the flat $\boldsymbol{\rho}_S=\boldsymbol{\rho}_t$ presented in Fig. 2(e). The final step is to acquire the surface LDOS from the $\boldsymbol{\rho}_{S,t}(V)$ obtained by Eq. (8) and then divided by $\boldsymbol{\rho}_t$. The recovered (black and red) LDOS for two separations together with the generated-input (green) $\boldsymbol{\rho}_S(V)$ curves are presented in the panels (d) of Fig. 3. Black spectra correspond to z_1 and red to z_2. Solid and dashed lines are the products $\boldsymbol{\rho}_{S,t}(V)/\boldsymbol{\rho}_t(0)$ and $\boldsymbol{\rho}_{S,t}(V)/\boldsymbol{\rho}_t(-V)$, respectively. Both products give very similar results for flat $\boldsymbol{\rho}_t(V)$ background with metal [see Fig. 3, (Id)] and semiconductor [see Fig. 3, (IId)] surfaces. The significant difference in the two products is in the case of parabolic $\boldsymbol{\rho}_t(V)$ background [see Fig. 3, (IIId)] where division by $\boldsymbol{\rho}_t(0)$ leads to a better recovery in the positive-bias range while division by $\boldsymbol{\rho}_t(-V)$ recovers the surface LDOS better in the negative-bias range. Also important is the result on the metal surface [see Fig. 3, (Id)] where the corrugation at negative biases corresponds to the tip and at positive biases reflects the surface illustrating the symmetric nature of the tunneling process. The overestimated amplitudes of negative part of the recovered spectra [see Fig. 3, (Id)] in comparison with the $\boldsymbol{\rho}_t(V)$ generated input [see Fig. 3, (Ia)] are due to the approximations made in the LDOS recovery scheme.[11]

The results of these simulations can be summarized in good agreement with the results in Ref. 11 as follows. (i) In all cases the $\Delta R_{1,2}$ method provides a topographic map with local minimum sufficient to estimate the Φ and z_0 parameters. The method has optimal accuracy in the positive-bias range where no β correction is needed and outside the surface states area which could have z dependence in some cases (see the field effect in part B of Sec. V).

(ii) The spectra obtained by the Φ^* method reflect predominantly the surface LDOS features for the $\boldsymbol{\rho}_S<\boldsymbol{\rho}_t$ case. One should note that it is applicable only for surfaces with nonzero DOS at the Fermi energy. (iii) The z^* method provides spectra dominated by the tip LDOS structure and can be used for the separation determination only when the probe has monotonic and featureless DOS. (iv) For metal surfaces the tip LDOS features dominate the negative-bias part of the recovery product with increased amplitude whereas the surface LDOS dominates the positive part and shows well-recovered amplitudes. (v) For semiconductor samples the recovered product is always dominated by the surface LDOS. (vi) The surface LDOS is best recovered when obtained from the $\boldsymbol{\rho}_{S,t}(V)/\boldsymbol{\rho}_t(-V)$ product for negative sample biases and from the $\boldsymbol{\rho}_{S,t}(V)/\boldsymbol{\rho}_t(0)$ product for positive sample biases. (vii) For the correct LDOS recovery at high negative biases a $\beta=f(z,\Phi,V)$ function is needed instead of constant $\beta=4$.

V. EXPERIMENTAL RESULTS

We now present two examples of variable-height scanning tunneling spectroscopy and LDOS recovery on metal and semiconductor surfaces mounted on a dual sample holder that allows measurements with the same tip without the need for sample exchange.

A. Polycrystalline Pt surface

The first experimental example is on polycrystalline Pt layer evaporated on a Ta foil [see Fig. 1(b)]. A tungsten tip was inked[14] with Pt after which spectroscopic measurements were performed on a nonmodified area of the Pt surface. All experimental data on the metal surface are presented as solid lines in Fig. 4. Figures 4(a) and 4(b) contain tunneling currents and their bias derivatives taken with set point z_0 at 100 pA and 2 V. $\Delta z(V)$ was programmed to be constant 0.3 Å while variable $\Delta z_1(V)$ and $\Delta z_2(V)$ were applied and are plotted in the top part of panel (a) in Fig. 4 with black and red curves, respectively. The $\Phi^*(V)$ and $\Phi_A(V)$ spectra were then obtained from the data in Figs 4(a) and 4(b) and are shown in Fig. 4(c). The $\Phi_A(V)$ spectrum diverges significantly approaching zero bias corresponding to the fact that $I(z_2)$ reaches the experimental detection limit and becomes zero at higher bias values then $I(z_1)$. In contrast $\Phi^*(V)$ saturates at a specific value at $V=0$ and was used to determine the tunneling barrier $\Phi=5.35$ eV. This value is reasonable for a Pt tip and Pt sample. Using this barrier value in Eq. (11) we calculated the $z^*(V)$ spectrum [see Fig. 4(d)]. The spectrum is strongly corrugated preventing any application of a low-order polynomial fit for the z_0 extrapolation at $V=0$. The z^* results also indicate that this particular probe has DOS which is not featureless. We overcome this obstacle by applying the $\Delta R_{1,2}$ method as in Fig. 2(e). The resulting $\Delta R_{1,2}$ (0.5 V) map is plotted in Fig. 4(f) showing a local minimum at $z_0=8$ Å and $\Phi=5.35$ eV which supports the Φ^* result in Fig. 4(c). The product $R_{1,2}(V)=\boldsymbol{\rho}_{S,t}(V,z_1)/\boldsymbol{\rho}_{S,t}(V,z_2)$ for $z_0=8$ Å and $\Phi=5.35$ eV is plotted in Fig. 4(e) and is close to the expected value of 1 [from Eq. (9)] over most of the bias range. The latter gives us confidence that the estimated parameters $\mathbf{\Phi}$ and z_0 are reasonably close to the actual values. Additionally, these parameters applied in Eq. (8) lead to a very good overlap of the recovered $\boldsymbol{\rho}_{S,t}(z_1)$ and $\boldsymbol{\rho}_{S,t}(z_2)$ spectra which can be seen in Fig. 4(g) plotted with black and red solid curves. The supplemental material[16] contains an analysis of $I(z)$ measurement that independently confirm the absolute separation and estimated barrier height.

B. Si(100)-(4×2) surface

Figure 5 shows data for the Si(100)-(4×2) surface where the solid lines represent VH-STS experimental results recorded on top the Si dimer row with a z_0 set point of 50 pA

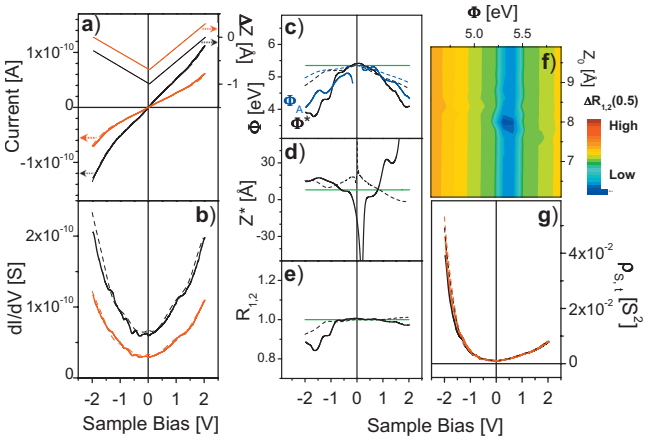

FIG. 4. (Color) VH-STS data and recovery scheme products for polycrystalline Pt surface and Pt-inked tip. The experimental results are plotted with solid black for z_1 and red for z_2 lines. The corresponding modeled data are shown with dashed curves with the same corresponding colors. The experimental set point z_0 is defined by the current of 100 pA and sample bias of 2 V. Tunneling currents and their bias derivatives are presented in (a) and (b), respectively. In (c) $\Phi^*(V)$, $\Phi_A(V)$, and $\mathbf{\Phi}$ are shown in black, blue, and green, respectively. The black curves in (d) are the $z^*(V)$ spectra and the green line is the z_0 estimate from the local minimum in (f). $\Delta R_{1,2}$ intensity map at 0.5 V with $\mathbf{\Phi}$ and z_0 as variable parameters is presented in (f). The corresponding $R_{1,2}(V)$ spectra for $\mathbf{\Phi}$ =5.35 eV and z_0=8 Å derived from the minimum in (f) are presented in (e). The combined tip and sample LDOSs recovered by the scheme are shown in (g).

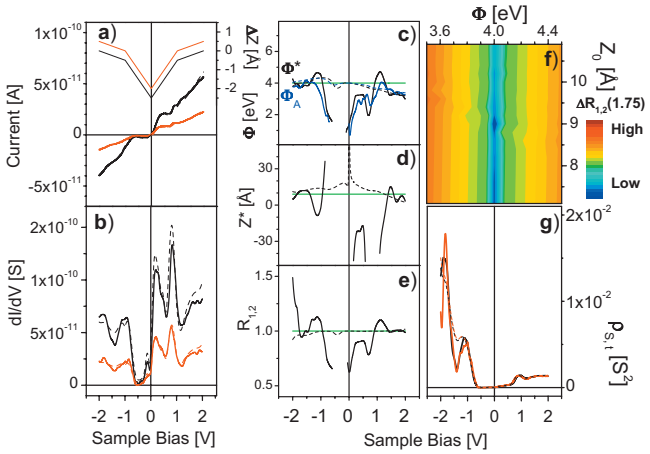

FIG. 5. (Color) VH-STS data and recovery scheme products for a Si(100)-(4×2) surface and Pt-inked tip. The experimental set point z_0 is defined by a current of 50 pA and sample bias of 2 V. The experimental results are plotted with solid black lines for z_1 and red lines for z_2. All corresponding modeled data are shown with dashed curves applying the same color coding. Tunneling currents and their bias derivatives are presented in (a) and (b), respectively. In (c) $\Phi^*(V)$, $\Phi_A(V)$, and $\mathbf{\Phi}$ are shown in black, blue, and green, respectively. The black curves in (d) are $z^*(V)$ spectra while with green the z_0 estimated from the local minimum in (f) is plotted. $\Delta R_{1,2}$ map at 1.75 V with $\mathbf{\Phi}$ and z_0 as variable parameters is shown in (f). The corresponding $R_{1,2}(V)$ spectra for $\mathbf{\Phi}$=4 eV and z_0=9 Å derived from the minimum in (f) are presented in (e). The combined tip and sample LDOSs recovered by the scheme are shown in (g).

and 2 V. The variable-height spectroscopy was performed with constant Δz=0.5 Å and the programmed $\Delta z_1(V)$ and $\Delta z_2(V)$ are shown on the top of panel (a) in Fig. 5, as black and red traces, respectively. Note that for both cases the tip approaches and retracts from the surface in a controlled manner as the bias is swept through the band-gap region. The simultaneously measured tunneling currents and their derivatives over the bias are presented in Figs. 5(a) and 5(b) and show a high signal-to-noise ratio over the entire bias range, which is the significant advantage of the present variable-height spectroscopy over constant-height measurements. The experimental barrier spectra in Fig. 5(c) are very intriguing. Both $\mathbf{\Phi}^*(V)$ (black line) and $\mathbf{\Phi}_A(V)$ (blue line) curves are observed to decrease in the ± 1 V region approaching values below 1 eV at V=0, such that it is impossible to estimate the actual tunneling barrier height based on these results. This is in striking contrast to the experimental results on the Pt surface [see Fig. 4(c)]. Additionally, extreme deviations are present in the $z^*(V)$ spectrum in the same bias region [black solid line in Fig. 5(d)] which exceed significantly the observed in Fig. 4(d) deviations due to the probe DOS. In order to clarify the source of these spectral behaviors in Fig. 6 we plotted the recovered $\boldsymbol{\rho}_{S,t}(V)$ data in logarithmic ordinate-scale together with the variation in the electric field $\Delta E_{field}(V)$ between the z_1 and z_2 experiments. Values of $\mathbf{\Phi}$ =4 eV and z_0=9 Å were used in Eq. (8) which were obtained by the $\Delta R_{1,2}$ method for bias of 1.75 V, which is well outside the ± 1 V region where these large extreme deviations are observed [see Fig. 5(f)]. A bias of 1.75 V was chosen since the experimental $R_{1,2}(V)$ curve in Fig. 5(e) is unity above 1.5 V and for which the $\Delta R_{1,2}$ (1.75) map in Fig. 5(f) reveals a local minimum at $\mathbf{\Phi}$=4 eV and z_0=9 Å. This approach continues to demonstrate very good consistency, similar to that found in the case of simulated data in Fig. 2(e) and for the Pt surface in Fig. 4(f). The supplemental material[16] contains an analysis of $I(z)$ measurement that independently confirm the absolute separation and the anomalous apparent barrier height.

Returning to Fig. 6, it is immediately evident that there is a lateral shift in the ± 1 V region between the black and red LDOS curves recovered at different heights. It is in this energy range that the Si surface states are located and given the variation in the electric field between the tip and sample in the two experiments we attribute this effect to a Stark shift of these surface states. The observed blueshift between $\boldsymbol{\rho}_{S,t}(z_2)$—red and $\boldsymbol{\rho}_{S,t}(z_1)$—black is indicated with blue arrows in Fig. 6. Thus the origin of the strong corrugation in the ± 1 V range observed in the experimental data shown in Figs. 5(c)–5(e) can be assign to this Stark effect, which is expected to be generally important in studies of semiconductor surface. It is also important to emphasize that the presence of strong deviations of the Φ^*, z^*, and $R_{1,2}$ spectra in the ± 1 V range does not prevent one from determining $\mathbf{\Phi}$ and z_0 using the high positive-bias region. The reasonable values of the latter parameters is manifested by the good overlap of the $\boldsymbol{\rho}_{S,t}(z_1)$ and $\boldsymbol{\rho}_{S,t}(z_2)$ curves plotted in the solid black and red lines in Fig. 5(g), respectively. This is an illustration of the benefits of having spectral data available over a wide ± 2 V bias range in one experiment when using variable-height spectroscopy.

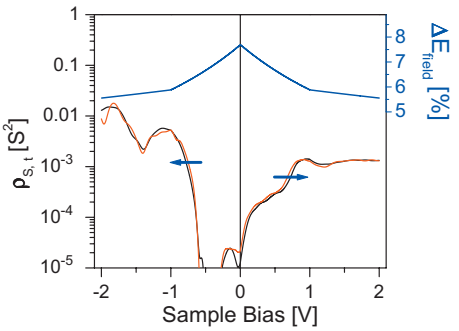

FIG. 6. (Color) Recovered combined tip and sample LDOS for a Si(100)-(4×2) surface with corresponding variation in the electric field during the VH-STS experiment. The recovered combined tip and sample LDOS is plotted in logarithmic ordinate (left) scale and shown in black for z_1 and red for z_2. The difference in the electric field between the tip and the surface for the two z_1 and z_2 ramps is plotted in blue and the corresponding ordinate is on the top right-hand side of the figure. Blue arrows indicated the blueshift of the LDOS curves with the increase in the electric field.

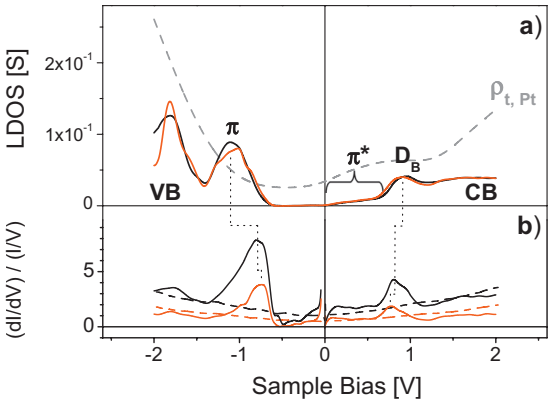

FIG. 7. (Color) Comparison of surface LDOS recovered by this scheme with that using $(dI/dV)/(I/V)$ (Ref. 2) normalization. Black is used to represent the results from z_1 data and red from z_2 data. (a) shows the recovered Si surface LDOS (solid lines) using this scheme together with the modeled Pt-inked tip LDOS which is plotted with grey dashed line. In (b) the corresponding $(dI/dV)/(I/V)$ spectra for the Si surface with solid lines and for the Pt surface with dashed lines are shown. The spectral feature assignment in (a) refers to the Si results. Dotted lines indicated the peak shifts between the recovered (a) and the normalized (b) Si spectra.

VI. MODELING OF EXPERIMENTAL RESULTS AND SURFACE DENSITY OF STATES RECOVERY

In order to obtain some estimate of the tip LDOS we used our observations from the simulation section of this study (Sec. IV) to model $\boldsymbol{\rho}_S(V)$ and $\boldsymbol{\rho}_t(V)$ (both of which are Pt metal) and to fit the experimental data in Fig. 4. The estimated (Φ and z_0) and programmed (Δz_1 and Δz_2) parameters from experiment were used unchanged. We tried to keep both densities as similar as possible reflecting their common material composition and no attempt was made to reproduce the fine structure in the experimental spectra. The focus was on the overall curve shapes and intensities. As we showed in Fig. 3, (IId) and (IIId), the fine structure of the tip LDOS has little or no influence on the recovered semiconductor surface LDOS so we can neglect it for the recovery of semiconductor surface density of states as described later.

The resulting $I(V)$ and $dI/dV(V)$ spectra obtained from modeled values of $\boldsymbol{\rho}_S(V)$ and $\boldsymbol{\rho}_t(V)$ [see later in Fig. 7 the exact $\boldsymbol{\rho}_t(V)$] for the Pt metal surface experimental data are presented in Fig. 4 as dashed lines. We achieved satisfactory agreement between the experimental and the modeled spectra of $I(V)$, $dI/dV(V)$, and $\boldsymbol{\rho}_{S,t}(V)$ which is demonstrated in Figs. 4(a), 4(b), and 4(g), respectively. For the Φ^* and Φ_A curves in Fig. 4(c) the agreement is good in the ± 1 V range while the deviation at high biases is due to the slight deviation at the same regions for the tunneling currents [see Fig. 4(a)] and consequently in the $dI/dV(V)$ results. In Fig. 4(d) apart form the high negative-bias region there is no agreement between the experiment and the simulated z^* spectra. This is a direct result of the fact that we did not include the tip LDOS fine structure in the modeling which has a major role in the $z^*(V)$ behavior as can be seen in the panels (c) in Fig. 3. Additionally, the $z^*(V)$ behavior is very sensitive to spectral noise which is always preset in experimental data. Despite the expected disagreement in panel (d) in Fig. 4, the overall agreement between experimental (solid lines) and modeled (dashed lines) spectra in the rest of the results in Fig. 4 gives us enough confidence that the modeled tip LDOS reflects the general shape and intensity of the Pt-inked probe used in our experiment and is sufficient to be used for the semiconductor case, namely, the Si(100) surface presented in the B part of the previous section.

Next we modeled the Si experimental results as in the Pt case. We used the already modeled tip LDOS form the Pt-surface experiment (see Fig. 4) and applied the estimated (Φ and z_0) and programmed (Δz_1 and Δz_2) parameters from the Si-surface experiment. We kept the $\boldsymbol{\rho}_t(V)$ unchanged and varied the $\boldsymbol{\rho}_S(V)$ features until a good agreement with experimental $I(V)$ and $dI/dV(V)$ spectra was obtained for both z_1 and z_2. The results of the modeling are presented as dashed curves in all panels in Fig. 5. The main observation is that the strong corrugation in the ± 1 V region of the Φ^*, z^*, and $R_{1,2}(V)$ spectra is removed for the modeled curves. This is a direct result of the fact that no Stark effect was included in $\boldsymbol{\rho}_S(V)$ between the z_1 and z_2 acquired spectra which confirms our conclusion. The good agreement between the experimental and modeled $\boldsymbol{\rho}_{S,t}(V)$ in Fig. 5(g) additionally confirms the reasonable estimate for the tunneling barrier and absolute separation values.

Finally, using the modeled Pt-tip LDOS plotted as dashed grey line in Fig. 7(a) we recovered the Si(100) surface LDOS which is presented also in Fig. 7(a) with black line for z_1 and red curve for z_2. The $\boldsymbol{\rho}_S(V)$ spectra were obtained from the $\boldsymbol{\rho}_{S,t}(V)/\boldsymbol{\rho}_t(-V)$ product for negative and from the $\boldsymbol{\rho}_{S,t}(V)/\boldsymbol{\rho}_t(0)$ product for positive sample biases based on the summary of our simulations at the end of Sec. IV. The filled $\boldsymbol{\pi}$ and empty $\boldsymbol{\pi}^*$ surface states of the Si(100)-(4×2) reconstruction of the sample can be identified. The localized character of the $\boldsymbol{\pi}$ state leads to a well-pronounced peak in the negative-bias range at the onset of the valence band while the delocalized character of the $\boldsymbol{\pi}^*$ state is observed as a low-intensity broad band below the conduction band and the strong Si-dimer back-bond (D_B).

For comparison the normalized conductance $(dI/dV)/(I/V)$ (Ref. 2) from the VH-STS experiment on the Si (solid lines) and the Pt (dashed curves) surfaces are presented in Fig. 7(b). No separation invariance is observed, namely, there is significant difference in both the intensity and peak positions for data recorded at different probe-sample separations [see z_1—black and z_2—red spectra in Fig. 7(b)] in contrast with the results of the present recovery scheme in Fig. 7(a). Additionally, all the central features of the $(dI/dV)/(I/V)$ spectra for the Si surface are artificially shifted toward the Si band-gap region. These two examples demonstrate the unreliability of the $(dI/dV)/(I/V)$ normalization[2] for the recovery of the correct LDOS especially on semiconductor samples.

VII. SUMMARY

We have introduced a variable-height scanning tunneling spectroscopy (VH-STS) which enables high signal-to-noise $I(V)$ and $dI/dV(V)$ spectra to be acquired over the entire measured bias range. We presented spectroscopic data taken in the ± 2 V bias range on two surfaces but with appropriately programmed $\Delta z(V)$ there are no limitations on the actual voltage range. We then introduced a LDOS recovery scheme based on the 1D-WKB approximation proposed by Koslowski *et al.*[10] and tested it on experimental data obtained using VH-STS on metal (Pt) and semiconductor (Si) surfaces with good results. The scheme generally recovers the combined tip and surface density of states and we introduced a method whereby the tip LDOS can be estimated using a probe inking and characterization method, thus allowing a determination of the surface LDOS. To implement this scheme certain parameters are required, namely, the tunneling barrier height and the absolute tip-surface separation, and we introduced three methods derived from the VH-STS to determine each of these parameters. The $\mathbf{\Phi}^*$ method gives accurate values of the barrier height on metal surfaces while on semiconductor samples significant deviation may occur due to Stark shift of the surface states or/and band banding. The $\mathbf{z}^*$ method for the absolute separation acquisition depends strongly on the tip LDOS and is expected to give accurate values only for flat probe density of states which was not the case for the Pt-inked tip used in this study. The $\Delta R_{1,2}$ method using the two recovered products from the VH spectroscopy for the parameters determination based on finding the local minimum in the $\mathbf{\Delta R_{1,2}}$ topographic map with $\mathbf{\Phi}$ and $\mathbf{z}$ as variables gives correct values in all cases, and is in addition supported by the approach to contact $I(z)$ experiments presented in the supplemental material[16] for the same probe and surfaces.

In conclusion the LDOS recovery scheme based on the 1D-WKB approximation is a reliable method applicable for all types of probes and surfaces investigated by scanning tunneling spectroscopy. Combined with VH-STS the scheme introduces three complimentary methods for tunneling barrier and absolute separation determination. This combination provides a very powerful surface science tool that enable rigorous LDOS information that directly complements the atomic-resolution capabilities of STM. We expect that this approach will find significant applications in wide areas of surface physics and chemistry.

ACKNOWLEDGMENT

This work was supported by Science Foundation Ireland under PI Award Grant No. 06/IN.1/I106.

*naydenob@tcd.ie

[1] G. Binnig, H. Rohrer, Ch. Gerber, and E. Weibel, Appl. Phys. Lett. **40**, 178 (1982).
[2] J. A. Stroscio, R. M. Feenstra, and A. P. Fein, Phys. Rev. Lett. **57**, 2579 (1986).
[3] For example, S. Modesti, H. Gutzmann, J. Wiebe, and R. Wiesendanger, Phys. Rev. B **80**, 125326 (2009).
[4] For example, J. Mysliveček, F. Dvořák, A. Stróżecka, and B. Voigtländer, Phys. Rev. B **81**, 245427 (2010).
[5] V. A. Ukraintsev, Phys. Rev. B **53**, 11176 (1996).
[6] N. Li, M. Zinke-Allmang, and H. Iwasaki, Surf. Sci. **554**, 253 (2004).
[7] B. Koslowski, C. Dietrich, A. Tschetschetkin, and P. Ziemann, Phys. Rev. B **75**, 035421 (2007).
[8] C. Wagner, R. Franke, and T. Fritz, Phys. Rev. B **75**, 235432 (2007).
[9] M. Passoni and C. E. Bottani, Phys. Rev. B **76**, 115404 (2007).
[10] B. Koslowski, H. Pfeifer, and P. Ziemann, Phys. Rev. B **80**, 165419 (2009).
[11] M. Passoni, F. Donati, A. L. Bassi, C. S. Casari, and C. E. Bottani, Phys. Rev. B **79**, 045404 (2009).
[12] M. Ziegler, N. Néel, A. Sperl, J. Kröger, and R. Berndt, Phys. Rev. B **80**, 125402 (2009).
[13] For examples, R. M. Feenstra, Surf. Sci. **603**, 2841 (2009); H. J. W. Zandvliet and A. van Houselt, Annu. Rev. Anal. Chem. **2**, 37 (2009).
[14] B. Naydenov, P. Ryan, L. C. Teague, and J. J. Boland, Phys. Rev. Lett. **97**, 098304 (2006); Nano Lett. **6**, 1752 (2006).
[15] J. B. Pethica and A. P. Sutton, J. Vac. Sci. Technol. A **6**, 2490 (1988).
[16] See supplementary material at http://link.aps.org/supplemental/10.1103/PhysRevB.82.245411 for verification of results from the article using approach to contact $I(z)$ measurements on the Pt and Si(100) surfaces using the same probe.